A NEW PROCEDURE FOR SIMULATING ACTIVE LATERAL FORCE IN SPATIALLY VARIABLE CLAY MODELED BY ANISOTROPIC RANDOM FIELD

Y.-G. Hu **J. Ching** *

Department of Civil Engineering
National Taiwan University
Taipei, Taiwan

ABSTRACT

A new procedure for simulating the active lateral force (P_a) is proposed for clays with anisotropic spatially variable undrained shear strength (s_u). With the proposed procedure, the P_a samples can be simulated without the use of the random field finite element method (*RFEM*). It requires only simple algebraic calculations and chart checking. Two retaining wall examples with isotropic or anisotropic random field are used to demonstrate the effectiveness of the proposed procedure.

Keywords: Soil spatial variability, Geotechnical engineering, Active lateral force, Anisotropic random field.

1. INTRODUCTION

Hu and Ching [1] explored the mechanism of the active lateral force (P_a) in clay when there is an isotropic spatial variability in the undrained shear strength (s_u). They showed that the effect of such spatial variability cannot be fully explained by pure spatial averaging and that the tendency of seeking the favorable failure path is also important. Ignoring the latter mechanism is unconservative. They further proposed a simplified procedure for simulating P_a under isotropic s_u random fields. However, this simplified procedure is limited to isotropic random fields and cannot handle anisotropic random fields, which are common in reality. This is because soil properties tend to be more variable in the vertical direction than in the horizontal direction [2]. Therefore, the main purpose of this study is to extend the work done by Hu and Ching [1] to anisotropic random fields and to propose a new procedure of simulating P_a under anisotropic s_u random fields. It will be made clear that this new procedure is able to effectively capture the complicated behaviors of P_a, such as the phenomenon of the critical scale of fluctuation (SOF) [1,3-7]. Two cases will be used to demonstrate the performance of the new procedure.

2. REVIEWS OF HU AND CHING [1]

This study is an extension of the aforementioned previous study [1]. Therefore, this previous study is reviewed briefly. The key concept in this previous work is the so-called "number of independent potential slip lines". This concept will be reviewed and will be shown to link to the tendency of seeking the favorable failure path. From here on, the term "potential slip line" is denoted by PSL.

2.1 Simulation of Active Lateral Force P_a

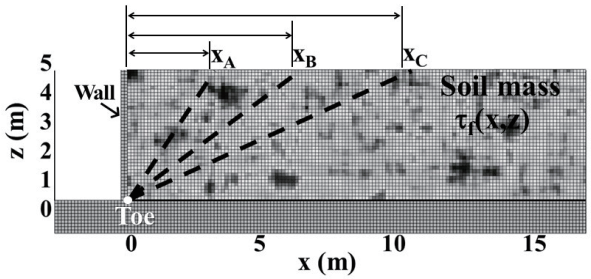
In Hu and Ching [1], a spatially variable undrained clay is considered. Therefore, the shear strength (τ_f) = the undrained shear strength (s_u). The undrained shear strength (s_u) at a point is denoted by $\tau_f(x, z)$, where x and z are the horizontal and vertical coordinates, respectively. The shear strength $\tau_f(x, z)$ is simulated as a stationary Gaussian random field with inherent mean $E(\tau_f) = \mu$ and inherent standard deviation $Var(\tau_f)^{0.5} = \sigma$. The COV of this random field is equal to σ/μ. To define the correlation structure of $\tau_f(x, z)$ between two locations with horizontal distance = Δx and vertical distance = Δz, the single exponential auto-correlation model is considered [8,9]:

$$\rho(\Delta x, \Delta z) = \exp\left(-\frac{2|\Delta x|}{\delta_x} - \frac{2|\Delta z|}{\delta_z}\right) \quad (1)$$

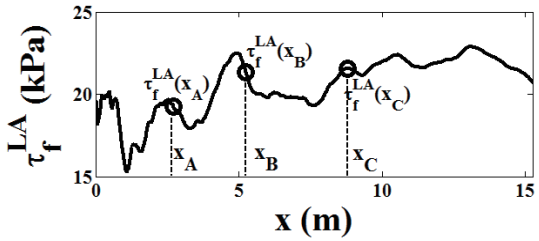
where δ_x and δ_z are the horizontal and vertical scales of fluctuation (SOFs). In Hu and Ching [1], only isotropic random fields are considered, *i.e.*, $\delta = \delta_x = \delta_z$. They proposed a process called "line search" to simulate a random sample of P_a using the limit equilibrium method (LEM). This process is illustrated in Fig. 1. Figure 1(a) shows a realization of the $\tau_f(x, z)$ isotropic random field, x_A, x_B, and x_C in Fig. 1(a) characterize the positions of the three potential slip lines (PSLs). They are the x coordinates of the right-hand-side end points of the three PSLs. It is assumed that the slip curves

* Corresponding author (jyching@gmail.com)

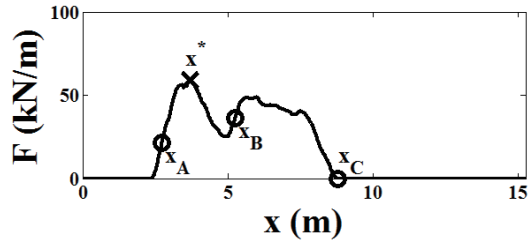
DOI : 10.1017/jmech.2015.5
Copyright © 2015 The Society of Theoretical and Applied Mechanics, R.O.C.
https://doi.org/10.1017/jmech.2015.5 Published online by Cambridge University Press



(a) Realization of the $\tau_f(x, z)$ random field



(b) 1D random field of $\tau_f^{LA}(x)$



(c) F(x) function

Fig. 1 Process of simulating a random sample of P_a using the LEM.

are straight lines. This assumption is in principle unconservative, but the actual effect of this assumption is minimal [1]. The "line average" along each *PSL* can be directly simulated by the Fourier series method [10] (see Eq. (19) in [10]). This line average is denoted by $\tau_f^{LA}(x)$. Using force equilibrium, it is shown that [1]

$$P_a = \max_x F(x) = \max_x \left(\frac{1}{2}\gamma H^2 - \tau_f^{LA}(x) \cdot \frac{x^2 + H^2}{x} \right) \quad (2)$$

where F is the lateral force from the wall required to support the failing soil mass (F depends on x); H is the wall height; γ is the soil unit weight. For each PSL with a position x, force equilibrium can be used to derive the lateral force F required to support the failing soil mass. Each PSL produces a "line average" τ_f^{LA}. The position x at which F(x) is maximized is denoted by x^*, which is the position of the critical slip line. The wedge above the critical slip line exerts the maximum lateral force to the wall, among all PSLs. This position x^* will be denoted by the "critical position". For homogeneous undrained clays, this critical position x^* is equal to the wall height H, because the inclination angle of the classical critical slip line is 45°. For spatially variable clays, x^* becomes random. However, Hu and Ching [1] showed that x^* cannot dramatically deviate from the classical value H, *i.e.*, $x^* \approx H$, because the critical slip line still needs to observe certain mechanical rules. The P_a shown in Eq. (2) is the active lateral force simulated by the line search method using the LEM. Let the "mobilized" shear strength, denoted by τ_f^m, be the τ_f^{LA} value along the critical slip line. It is the shear strength actually exhibited by the spatially variable clay behind the retaining wall. Therefore

$$P_a = \frac{1}{2}\gamma H^2 - \tau_f^m \cdot \frac{x^{*2} + H^2}{x^*} \quad \text{or}$$
$$\tau_f^m = \left(\frac{1}{2}\gamma H^2 - P_a \right) \Big/ \left(\frac{x^{*2} + H^2}{x^*} \right) \quad (3)$$

Note that different realizations of the random fields will produce different P_a and τ_f^m samples.

2.2 Independent PSLs

The independence between two PSLs is defined in Hu and Ching [1]. If the τ_f^{LA} values of two PSLs are independent, these two PSLs are said to be independent. Hu and Ching [1] showed that two PSLs can be independent even if they are close together. This can happen when the SOFs ($\delta = \delta_x = \delta_z$) are small. The critical slip line will locally seek among the independent PSLs to find the critical failure path that maximizes the lateral force F. If there are many mutually independent PSLs (these PSLs have mutually independent τ_f^{LA} values), the $\tau_f^{LA}(x)$ and F(x) functions will change dramatically with x. Hence, the tendency of seeking (*i.e.*, finding a maximum in the F(x) function) is high. They further showed that the "number of independent PSLs", denoted by n later on, can be effectively estimated using the following equation:

$$n \approx (0.112 + 0.871 \times COV) \times (\delta / H)^{-0.894} + 1 \quad (4)$$

With the above equation (Eq. (4)), *n* can be estimated based on the knowledge of H, COV (= σ/μ) and δ ($\delta_x = \delta_z$). Equation (4) is effective for isotropic cases.

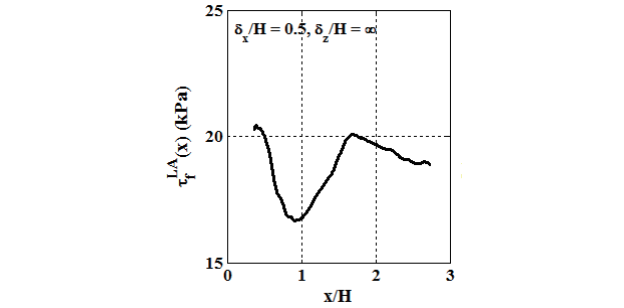
2.3 Equation (4) Not Applicable to Anisotropic Cases

Although Eq. (4) is effective for isotropic cases, it cannot handle anisotropic random fields ($\delta_x \neq \delta_z$). For anisotropic cases, an "equivalent" isotropic scale of fluctuation can be derived from δ_x and δ_z [11]:

$$\delta_E \approx \left[\cos(45°) / \delta_x + \sin(45°) / \delta_z \right]^{-1} \quad (5)$$

This δ_E is in fact the scale of fluctuation along the classical 45° PSL. It is the SOF that is actually "felt" by the anisotropic case. It is tempting to say that n for such an anisotropic case can be estimated by replacing δ in Eq. (4) by δ_E. However, this approach does not work well. Consider three anisotropic cases: (a) $\delta_x / H = 0.5$ and $\delta_z / H = \infty$; (b) $\delta_x / H = 1$ and $\delta_z / H = 1$; and (c) $\delta_x / H = \infty$ and $\delta_z / H = 0.5$. It is clear that these three

https://doi.org/10.1017/jmech.2015.5 Published online by Cambridge University Press



(a) $\delta_x / H = 0.5$ and $\delta_z / H = \infty$

(b) $\delta_x / H = 1$ and $\delta_z / H = 1$ (c) $\delta_x / H = \infty$ and $\delta_z / H = 0.5$

Fig. 2 $\tau_f^{LA}(x)$ functions for these anisotropic cases.

cases have identical δ_E (*i.e.*, $\delta_E / H = 0.707$), so it is "expected" to see the same degree of changes in their $\tau_f^{LA}(x)$ functions. Nevertheless, the degrees of changes in the $\tau_f^{LA}(x)$ functions for these three cases are quite different (see Fig. 2): case (a) is associated with the most severe change, whereas case (c) is associated with no change (constant). In general, Eq. (4) with the equivalent SOF δ_E cannot handle anisotropic random fields.

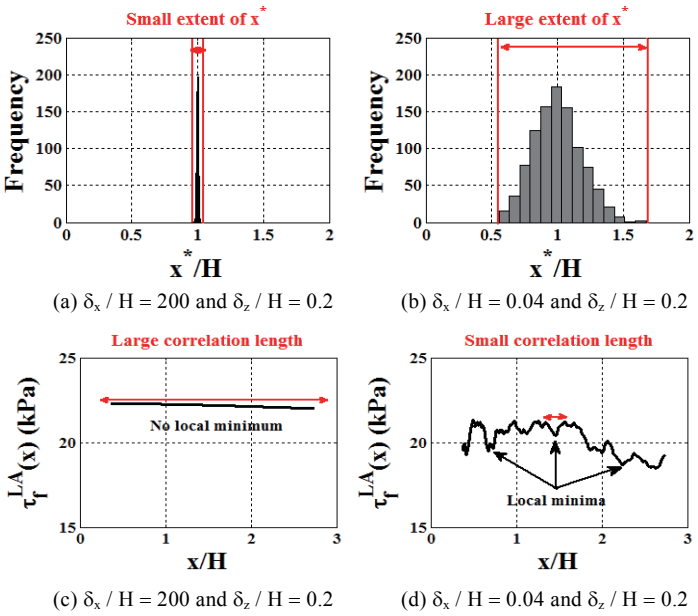
3. THE NUMBER OF INDEPENDENT POTENTIAL SLIP LINES (n)

It has been shown that Eq. (4) cannot successfully quantify the number of independent PSLs (n) for anisotropic cases. In this section, a method that is effective in estimating n for anisotropic cases is proposed. Many of the upcoming discussions will be given for anisotropic cases with $\delta_z / H = 0.2$ for simplicity and clarity, although the final conclusion is not limited to this anisotropic case. The most important observation is that the number of independent PSLs (n) should be related to the following two factors:

1. The extent of the critical position x^*. The position of the critical slip line x^* is not a prescribed position, because the critical slip line will locally seek the favorable failure path to maximize F. In fact, x^* varies around its classical value $x^* = H$. The length for the interval where x^* can occur is called its "extent". For instance, if x^* varies between H – 1m and H + 2m, the extent is 3m. The extent of x^* governs the length of the interval where the critical slip line can take place. Intuitively, the number of independent PSLs (n) should be proportional to this extent. In the extreme that the extent is zero, there can be only a single independent PSL (n = 1), namely, no seeking. This can happen when SOFs are large (homogeneous). In this case, x^* will be very close to its classical value H, and the extent is zero (no seeking). This is exemplified in Fig. 3(a) for a case with very large δ_x ($\delta_x / H = 200$). For another case with smaller δ_x ($\delta_x / H = 0.04$), the extent of x^* is larger. As mentioned earlier, the number of the independent PSLs (n) should be proportional to the extent. In a later subsection, numerical evidences will show that the x^* extent is roughly proportional to the "local variability" of the $\tau_f^{LA}(x)$ function, denoted by Δ. Moreover, one can use the Δ chart developed in the subsection (Fig. 6) to easily determine the value of Δ based on δ_x / H and δ_z / H.
2. Correlation length of $\tau_f^{LA}(x)$. The correlation length of $\tau_f^{LA}(x)$, denoted by θ, governs the degree of changes in the $\tau_f^{LA}(x)$ function. When θ is very large, $\tau_f^{LA}(x)$ will be a slowly changing function without local minimum. This is exemplified in Fig. 3(c) for a case with very large δ_x ($\delta_x / H = 200$). For another case with smaller δ_x ($\delta_x / H = 0.04$) in Fig. 3(d), $\tau_f^{LA}(x)$ is a quickly changing function, because θ is smaller. There are lots of local minima for this case. The local minima in $\tau_f^{LA}(x)$ usually correspond to the local maxima in the lateral force F(x). These local minima in $\tau_f^{LA}(x)$ or maxima in F(x) correspond to the possible failure paths. Hence, a large θ implies very few possible failure paths (tendency of seeking is low), and a small θ implies many possible failure paths (tendency of seeking is high). Intuitively, the number of the independent PSLs (n) should be proportional to 1/θ. In a later subsection, the detailed steps for calculating θ are presented. Moreover, one can use the θ chart developed in the subsection (Fig. 7) to easily determine the value of θ based on δ_x / H and δ_z / H.

It must be emphasized that n depends on both the correlation length (θ) and the local variability (Δ) of $\tau_f^{LA}(x)$, not on θ alone. The latter view (n depends on θ alone) can be derived from a one-dimensional (1D) random field: The number of "independent blocks" should only depend on its correlation length, not on its variability (*e.g.*, standard deviation). While this view is correct for 1D random fields, this view is incorrect for the retaining wall problem. Here we give a retaining wall example with very small θ, and yet its *n* value is very small (close to 1). Consider a retaining wall case with very small SOFs $\delta_x = \delta_z \approx 0$. It is clear that θ is very small for this case (see the red line in Fig. 7). According to the 1D random field intuition, its n should be large (lots of independent blocks). But, such a case with $\delta_x = \delta_z \approx 0$ resembles a homogeneous case. As a result, the critical slip line will have an inclination angle that is very close to 45°. Hence, there is only a single independent PSL (n = 1) for this case because the critical slip line is fixed at 45°: The 1D random field intuitive is incorrect. This example demonstrates that

https://doi.org/10.1017/jmech.2015.5 Published online by Cambridge University Press



(a) $\delta_x / H = 200$ and $\delta_z / H = 0.2$ (b) $\delta_x / H = 0.04$ and $\delta_z / H = 0.2$

(c) $\delta_x / H = 200$ and $\delta_z / H = 0.2$ (d) $\delta_x / H = 0.04$ and $\delta_z / H = 0.2$

Fig. 3 Histograms of x^* random field and the variation of τ_f^{LA} with respect to x for a realization of the $\tau_f(x, z)$.

n should not depend on θ alone, but also on the extent of x^*, which is proportional to Δ. In fact, for this case n = 1 because the x^* extent is zero.

3.1 Quantification of x^* Extent

Numerical evidences show that the x^* extent is roughly proportional to the "local variability" of the $\tau_f^{LA}(x)$. The x^* extent is characterized by its sample standard deviation, denoted by σ_{x^*}. For instance, $\sigma_{x^*} \approx 0$ if x^* is nearly deterministic ($\approx H$). This can happen when SOFs are very large. On the other hand, σ_{x^*} can be large if x^* is highly variable. The local variability of $\tau_f^{LA}(x)$ (near x = H) is defined to be the standard deviation of the difference between the $\tau_f^{LA}(x)$ values for the two PSLs with inclination angles = 40° and 50° (see Fig. 4):

$$\Delta = \text{stdev}\left[\tau_f^{LA}(x_R) - \tau_f^{LA}(x_L)\right] \quad (6)$$

where $x_R = H \times \cot(40°)$ and $x_L = H \times \cot(50°)$ are the x positions for the two PSLs. The two PSLs in Fig. 4 are around the classical slip line with inclination angle = 45°. Note that the unit of Δ is in kPa. As shown below, Δ can be derived analytically.

Let us denote these two PSLs by PSL_R and PSL_L and denote their lengths by L_R and L_L (Fig. 4). We further denote the SOFs along PSL_R and PSL_L by δ_R and δ_L, respectively. From [13],

$$\delta_R \text{ or } \delta_L = \left[\cos(40° \text{ or } 50°)/\delta_x + \sin(40° \text{ or } 50°)/\delta_z\right]^{-1} \quad (7)$$

It is clear that

$$\Delta^2 = \text{Var}\left[\tau_f^{LA}(x_R) - \tau_f^{LA}(x_L)\right] = \text{Var}\left[\tau_f^{LA}(x_R)\right] + \text{Var}\left[\tau_f^{LA}(x_L)\right] - 2\text{COV}\left[\tau_f^{LA}(x_R), \tau_f^{LA}(x_L)\right] \quad (8)$$

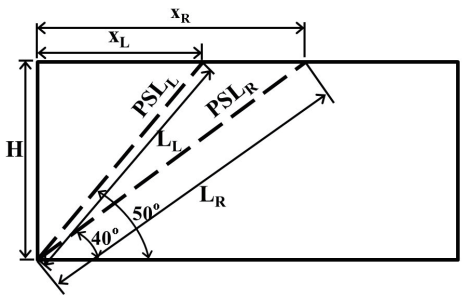


Fig. 4 Schematic of two PSLs, PSL_R and PSL_L.

where Var[·] and COV[·,·] denote the variance and covariance, respectively. Moreover,

$$\text{Var}\left[\tau_f^{LA}(x_R)\right] = \Gamma^2 \times \text{Var}\left[\tau_f(x, z)\right] = \sigma^2 \times \left(\left[2n_R - 1 + \exp(-2n_R)\right]/2n_R^2\right) \quad (9)$$

where $n_R = L_R / \delta_R$ is the equivalent number of SOFs along PSL_R. The same equation applies to $\text{Var}[\tau_f^{LA}(x_L)]$ by replacing n_R with $n_L = L_L / \delta_L$. The covariance can be computed by the following integration:

$$\text{COV}\left[\tau_f^{LA}(x_R), \tau_f^{LA}(x_L)\right] = \sigma^2 \int_0^1 \int_0^1 \exp\left(-\frac{2}{\delta_x} \times |x_R \times t_R - x_L \times t_R| - \frac{2H}{\delta_z} \times |t_R - t_L|\right) dt_R\, dt_L \quad (10)$$

where $t_R, t_L \in [0,1]$ are the local coordinates along PSL_R and PSL_L. The above integral can be solved by numerical integration.

Numerical evidences show that σ_{x^*} is roughly proportional to Δ. Note that σ_{x^*} and Δ have different units: the former is in meters, and the latter is in kPa. Therefore, it is more sensible to compare σ_{x^*} / H with Δ/μ. Figure 5 shows that σ_{x^*} / H and Δ/μ are roughly proportional for 100 cases in a wide range of values for H, μ, COV, δ_x, and δ_z. Because n is expected to be proportional to σ_{x^*}, n should be also roughly proportional to Δ.

It turns out that there is a unique mathematical relationship between Δ/σ and $(\delta_x / H, \delta_z / H)$, and Fig. 6 shows this unique relationship. From Fig. 6, Δ/σ can be determined given the information on $(\delta_x / H, \delta_z / H)$. The red line in Fig. 6 represents the results for isotropic random fields ($\delta = \delta_x = \delta_z$).

3.2 Calculation of θ

This subsection discusses the detailed steps for calculating θ, the correlation length in $\tau_f^{LA}(x)$. The notion of "correlation length" [14] is adopted here for $\tau_f^{LA}(x)$, rather than the SOF for $\tau_f^{LA}(x)$, because the SOF of $\tau_f^{LA}(x)$ is infinity. This is because even if two PSLs have remote positions x_R and x_L, $\tau_f^{LA}(x_R)$ and $\tau_f^{LA}(x_L)$ may be still slightly positively correlated because both lines need to pass through the same toe region (see Fig. 1(a)). However, the correlation length is defined differently from the *SOF*: the latter is defined

https://doi.org/10.1017/jmech.2015.5 Published online by Cambridge University Press

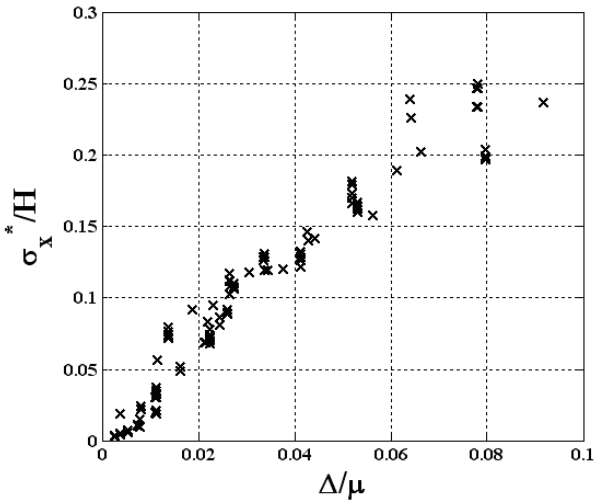


Fig. 5 Relationship between σ_{x^*}/H and Δ/μ.

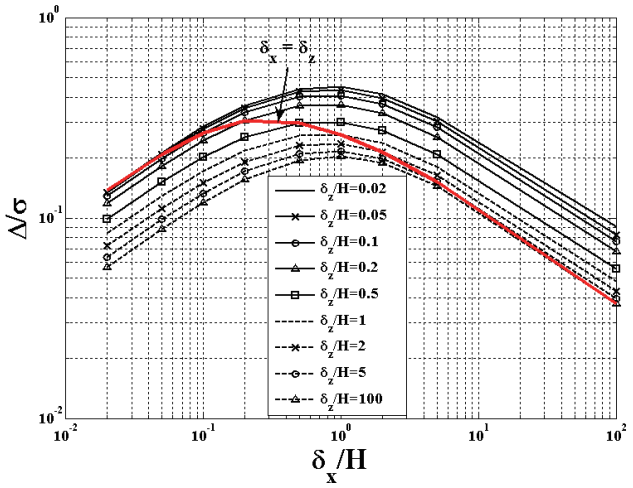


Fig. 6 Relationships between Δ/σ and (δ_x / H, δ_z / H).

to be the total area under the auto-correlation function, whereas the former is defined to be the interval length at which the correlation coefficient is exactly exp(−1) [14]. Again, consider PSL_R and PSL_L with locations x_R and x_L, and denote their line averages by $\tau_f^{LA}(x_R)$ and $\tau_f^{LA}(x_L)$. If the correlation coefficient between $\tau_f^{LA}(x_R)$ and $\tau_f^{LA}(x_L)$ is exactly equal to exp(−1), the correlation length for $\tau_f^{LA}(x)$ is simply the interval length $x_R - x_L$. For our purpose, x_R and x_L should be centered at H. We adopt $x_R = H \times r$ and $x_L = H/r$ ($r > 1$). The ratio r should satisfy

$$\rho\left[\tau_f^{LA}(H\times r), \tau_f^{LA}(H/r)\right] = \exp(-1) \tag{11}$$

where $\rho(\cdot,\cdot)$ denotes the correlation coefficient. Let us denote the lengths of PSL_R and PSL_L by L_R and L_L, respectively. Also denote the SOFs along PSL_R and PSL_L by δ_R and δ_L, respectively. δ_R and δ_L can be determined using Eq. (8). It can be shown that

$$\rho\left[\tau_f^{LA}(H\times r), \tau_f^{LA}(H/r)\right] = \frac{\int_0^1\int_0^1 \exp\left(-\frac{2}{\delta_x}\left|H\times r\times t_R - \frac{H}{r}\times t_L\right| - \frac{2}{\delta_z}\times H\times|t_R - t_L|\right) dt_R dt_L}{\sqrt{\left[2n_R - 1 + \exp(-2n_R)\right]/2n_R^2}\times\sqrt{\left[2n_L - 1 + \exp(-2n_L)\right]/2n_L^2}} \tag{12}$$

where t_R, $t_L \in [0,1]$ are the local coordinates along PSL_R and PSL_L, respectively, and $n_R = L_R/\delta_R$ and $n_L = L_L/\delta_L$ are the equivalent numbers of SOFs along PSL_R and PSL_L, respectively. The r value that satisfies Eq. (11) is first solved, then θ is simply $H \times r - H/r$. There is a unique mathematical relationship between θ/H and (δ_x / H, δ_z / H). From Fig. 7, θ/H can be determined based on (δ_x / H, δ_z / H) without referencing the detailed calculations. n is expected to be proportional to 1/θ.

In summary, we proposed the above two factors to characterize the number of independent PSLs (n): (a) the local variability of $\tau_f^{LA}(x)$, denoted by Δ; and (b) the correlation length of $\tau_f^{LA}(x)$, denoted by θ. It is expected that *n* should be proportional to Δ and 1/θ. As a result, the following equation is proposed:

$$n \approx c\times\frac{\Delta/\mu}{\theta/H} + 1 \tag{13}$$

where c is a constant to be determined; μ is the (inherent) mean value of the $\tau_f(x, z)$ random field; Δ can be checked from Fig. 6; θ can be checked from Fig. 7. Note that the minimum value of n is 1, because there is at least a single independent PSL. This is why there is an extra term "1" in the above equation. In Eq. (13), Δ and θ are normalized by μ and H to remove the impacts of the problem size (H) and the inherent mean (μ) of the random field. The constant c will be calibrated later using LEM simulation results: the resulting c value is about 16.

Consider the following retaining wall example with δ_x = 5m, δ_z = 1m, H = 5m, μ = 20kPa, and COV = 0.3 (the inherent standard deviation σ = 20 × 0.3 = 6kPa). The following steps can be used to determine the number of independent PSLs (n):

1. Determine Δ/σ from Fig. 6 based on (H, δ_x, δ_z). The resulting Δ/σ = 0.366. Hence Δ/μ = (COV × Δ/σ) = 0.1098.
2. Determine θ/H from Fig. 7 based on (H, δ_x, δ_z). The resulting θ/H = 1.545.
3. Calculate $n = 16 \times (\Delta/\mu)/(\theta/H) + 1 = 2.14$.

This means that there are about 2.14 independent PSLs from which the critical slip line can choose from. The more the n value, the more the tendency of seeking.

3.3 Calibration of the Constant 'c' Using the Principle of Maximum Likelihood

Hu and Ching [1] demonstrated that it is possible to estimate the number of independent PSLs (n) based on the LEM simulation results. Corresponding to each P_a sample simulated by the line search method in the LEM,

https://doi.org/10.1017/jmech.2015.5 Published online by Cambridge University Press

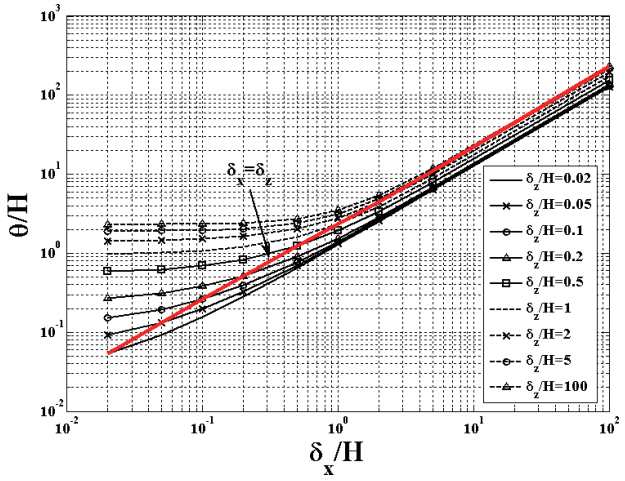


Fig. 7 Relationships between θ/H and (δ_x / H, δ_z / H).

there is a τ_f^m sample (see Eq. (3)). This τ_f^m is the line average along the critical slip line, $\tau_f^{LA}(x^*)$. Let us assume τ_f^m to be a minimum in the $\tau_f^{LA}(x^*)$ function in a local neighborhood of x ≈ H and that there are n independent PSLs within this neighborhood. Namely,

$$\tau_f^m = \min(\tau_f^{LA,1}, \tau_f^{LA,2}, ..., \tau_f^{LA,n}) \tag{14}$$

where ($\tau_f^{LA,1}$, $\tau_f^{LA,2}$, …, $\tau_f^{LA,n}$) are the line averages of the n independent PSLs. Because all PSLs cluster around the classical critical slip line, each τ_f^{LA} is normally distributed with mean value = μ and roughly the same variance = $\sigma^2 \times \Gamma^2$, where Γ^2 is the variance reduction factor due to the line average along the classical slip line. It can be shown that [9]

$$\Gamma^2 = \left[2L_p / \delta_p - 1 + \exp(-2L_p/\delta_p)\right] \Big/ \left(2L_p^2 / \delta_p^2\right) \tag{15}$$

where $L_p = 2^{0.5} \times H$ is the length of the classical slip line; δ_p is the SOF along the classical slip line;

$$\delta_p \approx \left[\cos(45°)/\delta_x + \sin(45°)/\delta_z\right]^{-1} \tag{16}$$

The probability density function (PDF) of τ_f^m has the following expression [1]

$$f(\tau) = \frac{n}{\sqrt{\sigma^2 \times \Gamma^2}} \times \left[1 - \Phi\left(\frac{\tau - \mu}{\sqrt{\sigma^2 \times \Gamma^2}}\right)\right]^{n-1} \times \varphi\left(\frac{\tau - \mu}{\sqrt{\sigma^2 \times \Gamma^2}}\right) \tag{17}$$

where Φ is the CDF of the standard normal random variable; φ is the PDF of the standard normal random variable; μ and σ^2 are the known inherent mean and inherent variance of the $\tau_f(x, z)$ random field, respectively.

Given the τ_f^m samples simulated by the LEM of a sample size N (denoted by $\tau_{f,1}^m$, $\tau_{f,2}^m$, …, $\tau_{f,N}^m$), n can be estimated through the maximum likelihood (ML) method: The best estimate of n is the one that maximizes the following likelihood function L(n):

$$L(n) = \prod_{i=1}^{N} \left(\frac{n}{\sqrt{\sigma^2 \times \Gamma^2}} \times \left[1 - \Phi\left(\frac{\tau_{f,i}^m - \mu}{\sqrt{\sigma^2 \times \Gamma^2}}\right)\right]^{n-1} \times \varphi\left(\frac{\tau_{f,i}^m - \mu}{\sqrt{\sigma^2 \times \Gamma^2}}\right) \right) \tag{18}$$

where $\tau_{f,i}^m$ is the i th simulated τ_f^m sample. The estimation of n is demonstrated for the two anisotropic cases: (a) δ_x / H = 200 and δ_z / H = 0.2; (b) δ_x / H = 0.04 and δ_z / H = 0.2. Both cases have inherent mean μ = 20kPa, H = 5m, and COV = 0.3. Figure 8 shows the histograms of 1000 τ_f^m samples simulated by the LEM. For the case with large δ_x (δ_x / H = 200), the mean value of the simulated τ_f^m is close to the inherent mean 20kPa (see Fig. 8(a)). The $\tau_f^{LA}(x)$ function is nearly constant for this case, hence nearly no tendency of seeking. The above ML method gives n = 1.00. The solid line in Fig. 8(a) plots the PDF of τ_f^m (Eq. (17)) with n = 1.00. For the case with small δ_x (δ_x / H = 0.04), the mean value of the simulated τ_f^m is smaller than the inherent mean 20kPa (see Fig. 8(b)). The tendency of seeking is strong. The above ML method gives n = 3.82. The solid line in Fig. 8(b) plots the PDF of τ_f^m (Eq. (17)) with n = 3.82.

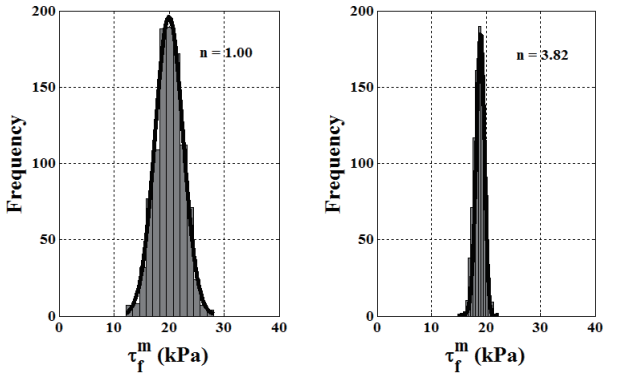
Figure 9 shows the n versus (Δ/μ)/(θ/H) plot for 200 retaining wall cases with a wide range of H, μ, COV, δ_x, and δ_z (H = 3 ~ 20m, μ = 10 ~ 50kPa, COV = 0.1 ~ 0.3, δ = 0.1 ~ 2000m). These cases include 50 isotropic cases (circles) and 150 anisotropic cases (crosses). For each case, 1000 samples of τ_f^m are simulated and used to estimate n using the ML method. The parameter (Δ/μ)/(θ/H) for each case is also calculated based on its COV, H, δ_x, and δ_z. It is found that Eq. (13) with c = 16 roughly holds (the solid line in Fig. 9).

4. A NEW PROCEDURE OF SIMULATING P_a SAMPLES

With Eq. (13), n can be estimated based on (Δ/μ)/(θ/H) and P_a can be simulated without actually doing the more complicated LEM or the random field finite element method (RFEM). The following procedure is proposed in this study to simulate P_a samples (for ϕ = 0° condition). Unlike the procedure originally proposed in Hu and Ching [1] being limited to isotropic spatial variability, this new procedure applies to both isotropic and anisotropic random fields. It requires the knowledge of H, γ, μ, COV, δ_x, and δ_z and consists of the following steps:

1. Determine Δ/σ from Fig. 6 based on (H, δ_x, δ_z). Determine Δ/μ = (COV × Δ/σ).
2. Determine θ/H from Fig. 7 based on (H, δ_x, δ_z).
3. Calculate (Δ/μ)/(θ/H), and estimate n using Eq. (13).
4. Simulate a random sample U from a uniform distribution with the range of [0,1].
5. A sample of τ_f^m can be obtained as

https://doi.org/10.1017/jmech.2015.5 Published online by Cambridge University Press



(a) δ_x / H = 200 and δ_z / H = 0.2 (b) δ_x / H = 0.04 and δ_z / H = 0.2

Fig. 8 Histograms of the simulated $\tau_f{}^m$ samples.

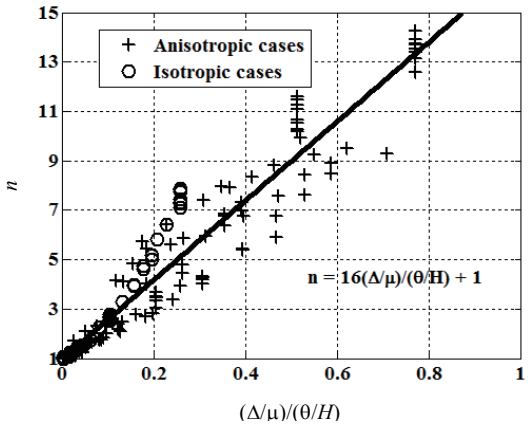


Fig. 9 n versus (Δ/μ)/(θ/H) relationship.

$$\tau_f^m = \mu + \sqrt{\sigma^2 \times \Gamma^2} \times \Phi^{-1}\left[1-(1-U)^{\left(\frac{1}{n}\right)}\right] \qquad (19)$$

where Φ^{-1} is the inverse CDF of the standard normal random variable; Γ^2 is the variance reduction factor and can be calculated using Eqs. (15) and (16).

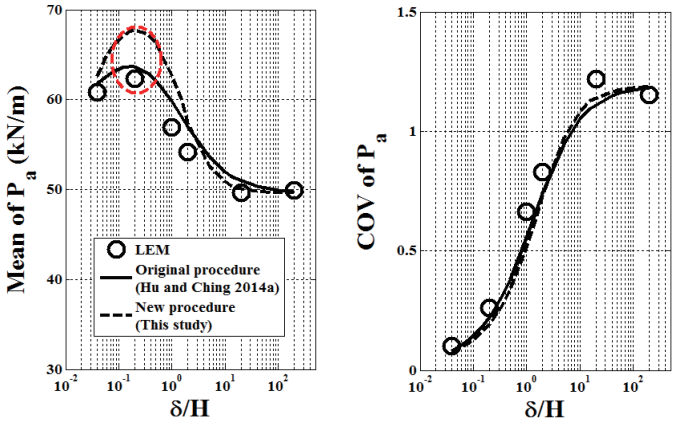
6. A sample of P_a can be obtained as

$$P_a = \frac{1}{2}\times\gamma\times H^2 - \tau_f^m \times \frac{x^{*2}+H^2}{x^*} \approx \frac{1}{2}\times\gamma\times H^2 - 2\times\tau_f^m\times H \qquad (20)$$

The approximation "≈" in this equation is due to the fact that x^* is typically around H, so $(x^{*2} + H^2)/x^* \approx 2 \times x^*$. This approximation is conservative because $(x^{*2} + H^2)/x^*$ reaches its minimum value at x^* = H, hence P_a reaches its maximum value at x^* = H.

Repeat the above Steps 4 ~ 6 N times to obtain N Monte Carlo simulation (MCS) samples of P_a.

The performance of the above new procedure is first illustrated using an isotropic case, in which H = 5m, γ = 20kN/m^3, μ = 20kPa, COV = 0.3, δ/H = δ_x / H = δ_z / H varies from 0.05 to 200. An anisotropic case will be examined later. The circles in Fig. 10 shows the sample mean and COV of P_a samples simulated by the LEM, *i.e.*, the line search method illustrated in Fig. 1. 600 samples of P_a are found to be sufficient to produce



(a) Mean of P_a with respect to δ/H (b) COV of P_a with respect to δ/H

Fig. 10 Variation of (a) the mean of P_a and (b) COV of P_a with respect to δ/H for an isotropic case with $\delta = \delta_x = \delta_z$.

stable sample mean and COV of P_a. Here, a sample size N = 1000 is adopted. The solid lines show the mean and COV of P_a predicted by the original procedure based on Eq. (4), proposed by Hu and Ching [1]. The dash lines in Fig. 10 show the mean and COV of P_a predicted by the new procedure proposed in this study. First of all, both the original and new procedures exhibit certain discrepancy to the LEM results. For the new procedure, this discrepancy is partly due to the discrepancy between the mean trend (solid line) and the data (circles & crosses) in Fig. 9. Another possible source for the discrepancy is the approximation "≈" in Eq. (20). Nonetheless, both the original and new procedures are able to effectively predict the variation of the mean and COV of P_a simulated by the LEM. However, the original procedure based on Eq. (4) is more accurate in predicting the P_a mean (the new procedure is more conservative). This is because the original procedure is specifically for isotropic cases, but the new procedure is more generic. Because the new procedure needs to fit to both isotropic and anisotropic cases, its fit to the isotropic cases is somewhat compromised. This can be seen from Fig. 9: The solid line (the fit by the new procedure) does not fit perfectly to the isotropic cases (circles) because it has to fit to all data points (circles and crosses).

The new procedure is able to capture the phenomenon of the critical SOF. In literature, there is sufficient numerical evidence [12] to show that complex non-classical failure mechanisms are produced when the SOF is comparable to some multiple of the characteristic length of the structure (*e.g.*, height of slope, diameter of tunnel, depth of excavation). This critical SOF is observed in other studies as well [1,3-7]. Hence, spatial variability affects geotechnical analysis in a manner that is more fundamental than variance reduction. The P_a simulated by the LEM exhibits the phenomenon of the critical SOF when δ/H is around 0.2 (see the dashed circle in Fig. 10(a)). It is clear that both the original and new procedures successfully capture this phenomenon of the critical SOF.

https://doi.org/10.1017/jmech.2015.5 Published online by Cambridge University Press

It is of interest to verify whether the new procedure is effective for anisotropic cases. Figure 11 show the results for a case with H = 5m, γ = 20kN/m^3, μ = 20kPa, COV = 0.3, δ_z / H is fixed at 0.5, but δ_x / H varies from 0.5 to 200. The new procedure is able to effectively predict the variation of the mean and COV of P_a simulated by the LEM. Note that the original procedure with Eq. (4) with an equivalent SOF is not successful for this anisotropic case. Two equivalent SOF*s* are examined: (a) The δ_E proposed by Vanmarcke [11] (Eq. (5)) and (b) The δ_E proposed by El-Ramly *et al.* [15]:

$$\delta_E \approx \sqrt{\delta_x \cdot \delta_z} \tag{21}$$

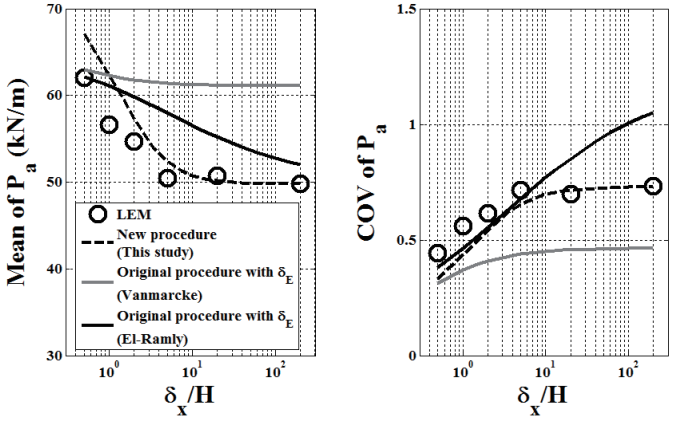
The black and gray lines in Fig. 11 show the mean and COV of P_a predicted by Eq. (4) with δ = the above two δ_E. It is clear that Eq. (4) with $\delta = \delta_E$ cannot effectively predict the variation of the mean and COV of P_a simulated by the LEM.

4.1 Consideration of a Tension Crack

The above new procedure of simulating P_a samples does not consider the existence of a tension crack. This tension crack issue has been addressed in Hu and Ching [1]. Based on their results, Eq. (2) should be altered into the following equation when a tension crack is present:

$$\begin{aligned} P_a &= \max_x F(x) \\ &= \max_x \left(\frac{1}{2}\gamma(H^2 - z_c^2) - \tau_f^{LA} \cdot \frac{(H - z_c)(x^2 + H^2)}{x \cdot H} \right) \end{aligned} \tag{22}$$

where $z_c = 2\mu/\gamma$ is the mean depth of the tension crack. It is clear when the tension crack is not considered (z_c = 0), Eq. (22) reduces to Eq. (2). The following modified procedure is proposed to simulate P_a samples to account for the presence of such a tension crack.



(a) Mean of P_a with respect to δ_x / H (b) COV of P_a with respect to δ_x / H

Fig. 11 Variation of (a) the mean of P_a and (b) COV of P_a with respect to δ_x / H for an anisotropic case with δ_z / H = 0.5.

1. Determine Δ/σ from Fig. 6 based on (H, δ_x, δ_z). Determine Δ/μ = (COV × Δ/σ).
2. Determine θ/H from Fig. 7 based on (H, δ_x, δ_z).
3. Calculate $(\Delta/\mu)/(\theta/H)$, and estimate n using Eq. (13).
4. Compute the mean depth of the tension crack $z_c = 2\mu/\gamma$.
5. Simulate a random sample U from a uniform distribution with the range of [0,1].
6. A sample of τ_f^m can be obtained as

$$\tau_f^m = \mu + \sqrt{\sigma^2 \times \Gamma^2} \times \Phi^{-1}\left[1 - (1 - U)^{\left(\frac{1}{n}\right)}\right] \tag{23}$$

where Γ^2 can be calculated using Eqs. (15) and (16), but L_p is shorter due to the presence of the tension crack: L_p is now equal to $2^{0.5} \times (H - z_c)$. The resulting Γ^2 is

$$\Gamma^2 = \frac{2(H - z_c)(\delta_x + \delta_z)/(\delta_x \delta_z) - 1 + \exp\left[-2(H - z_c)(\delta_x + \delta_z)/(\delta_x \delta_z)\right]}{2(H - z_c)^2(\delta_x + \delta_z)^2/(\delta_x^2 \delta_z^2)} \tag{24}$$

A sample of P_a can be obtained as

$$\begin{aligned} P_a &= \frac{1}{2}\gamma(H^2 - z_c^2) - \tau_f^{LA} \cdot \frac{(H - z_c)(x^{*2} + H^2)}{x^* \cdot H} \\ &\approx \frac{1}{2}\gamma \cdot (H^2 - z_c^2) - 2\tau_f^m \cdot (H - z_c) \end{aligned} \tag{25}$$

Again, the approximation "≈" in this equation is conservative.

Repeat the above Steps 3 ~ 5 N times to obtain N Monte Carlo simulation samples of P_a. The performance of this modified procedure that counts for the tension crack is also satisfactory. It can effectively predict the LEM results.

5. CONCLUSIONS

This study extends a previous work done by the authors [1] regarding simulating the active lateral force (P_a) samples when there is spatial variability in the clay behind a retaining wall. This previous work is applicable only to cases with isotropic spatial variability, but the current study extends it to anisotropic cases. The main contribution of this study is to characterize the tendency of seeking the favorable failure path using the number of independent potential slip lines (n), even under anisotropic random fields. It is proposed that n can be quantified by the following two factors: (a) The local variability of $\tau_f^{LA}(x)$ and (b) The correlation length of $\tau_f^{LA}(x)$. Moreover, the above two factors can be easily quantified by checking charts (Figs. 6 and 7). This chart checking does not require sophisticated analyses, such as the limit equilibrium method (LEM) and random field finite element method (RFEM). Finally, a new procedure is proposed to simulate the P_a samples under generic conditions, not limited to iso-

https://doi.org/10.1017/jmech.2015.5 Published online by Cambridge University Press

tropic spatial variability. The P_a samples simulated by the new procedure have statistics similar to those simulated by the LEM.

There are some limitations. The proposed method is only for clays. It should not be implemented to cases with cohesionless backfill soils. The possible friction between the wall and soil is also not studied, and the impact of such soil-wall interaction is not known. However, for general problems with cohesionless backfill soils and with possible structural interactions, the basic ideas of this study may still hold true. This study only considers the stationary Gaussian random field. Problems involving non-Gaussian random fields, such as lognormal random field, need further study.

ACKNOWLEDGEMENTS

This study was under the sponsorship of the Ministry of Science and Technology (MOST) of Republic of China, under the project 100-2628-E-002-040-MY3 & 103-2811-E-002-042. The authors would like to acknowledge such a gracious support from MOST.

NOMENCLATURE

F	:	lateral force
PSL	:	potential slip line
P_a	:	active lateral force
RFEM	:	random field finite element method
LEM	:	limit equilibrium method
H	:	wall height
γ	:	unit weight
ϕ	:	friction angle
c	:	cohesion
τ_f	:	shear strength
$\tau_f(x, z)$	:	the random field for τ_f
τ_f^{LA}	:	line average of $\tau_f(x, z)$ along a PSL
τ_f^m	:	mobilized shear strength
σ	:	inherent standard deviation of the $\tau_f(x, z)$ random field
μ	:	inherent mean of the $\tau_f(x, z)$ random field
COV	:	coefficient of variation
SOF	:	scale of fluctuation
δ_E	:	equivalent isotropic SOF
δ_p	:	SOF along the PSL
δ_x	:	horizontal SOF
δ_z	:	vertical SOF
β	:	inclination angle of the PSL
L_p	:	length of the PSL
Γ^2	:	variance reduction factor
ρ	:	auto-correlation
PDF	:	probability density function
N	:	sample size
Φ	:	CDF of the standard normal random variable
n	:	number of independent PSLs
n_p	:	equivalent number of SOFs along the PSL
φ	:	PDF of the standard normal random variable
θ	:	correlation length
Δ	:	standard deviation of $\tau_f^{LA}(x_R) - \tau_f^{LA}(x_L)$
L_x	:	horizontal dimension of the simulation domain
L_z	:	vertical dimension of the simulation domain
Δx	:	horizontal distance
Δz	:	vertical distance
x	:	horizontal coordinate
z	:	vertical coordinate
x^*	:	position of the critical slip line
σ_{x^*}	:	standard deviation of x^*

REFERENCES

1. Hu, Y. G. and Ching, J., "Impact of Spatial Variability in Undrained Shear Strength on Active Lateral Force in Clay," *Structural Safety*, **52**, pp. 121–131 (2015).
2. Phoon, K. K., "Reliability-Based Design of Foundations for Transmission Line Structures," Ph.D. Dissertation, Cornell University (1995).
3. Fenton, G. A. and Griffiths, D. V., "Bearing Capacity Prediction of Spatially Random *c*-φ Soils," *Canadian Geotechnical Journal*, **40**, pp. 54–65 (2003).
4. Breysse, D., Niandou, H., Elachachi, S. and Houy, L., "A Generic Approach to Soil-Structure Interaction Considering the Effects of Soil Heterogeneity," *Geotechnique*, **55**, pp. 143–150 (2005).
5. Fenton, G. A., Griffiths, D. V. and Williams, M. B., "Reliability of Traditional Retaining Wall Design," *Geotechnique*, **55**, pp. 55–62 (2005).
6. Soubra, A. H., Massih, Y. A. and Kalfa, M., "Bearing Capacity of Foundations Resting on a Spatially Random Soil," *GeoCongress: Geosustainability and Geohazard Mitigation (GSP 178)*, New Orleans Louisiana US, pp. 66–73 (2008).
7. Hu, Y. G. and Ching, J., "The Critical Scale of Fluctuation for Active Lateral Forces in Spatially Variable Undrained Clays," *Computers and Geotechnics*, **57**, pp. 24–29 (2014).
8. Vanmarcke, E. H., "Probabilistic Modeling of Soil Profiles," *Journal of Geotechnical Engineering Division*, ASCE, **103**, pp. 1227–1246 (1997)
9. Vanmarcke, E. H., *Random Fields: Analysis and Synthesis*, MIT Press, Cambridge, Massachusetts (1984).

https://doi.org/10.1017/jmech.2015.5 Published online by Cambridge University Press

10. Jha, S. K. and Ching, J., "Simulating Spatial Averages of Stationary Random Field Using Fourier Series Method," *Journal of Engineering Mechanics*, **139**, pp. 594–605 (2013).
11. Vanmarcke, E. H., "Reliability of Earth Slopes," *Journal of Geotechnical Engineering Division*, **103**, pp. 1247–1265 (1997).
12. Fenton, G. A. and Griffiths, D. V., *Risk Assessment in Geotechnical Engineering*, John Wiley & Sons, New York (2008).
13. Ching, J., Phoon, K. K. and Kao, P. H., "Mean and Variance for Mobilized Shear Strengths of Spatially Variable Soils under Uniform Stress States," *Journal of Engineering Mechanics*, **140**, pp. 487–501 (2014).
14. Li, C. and Der Kiureghian, A., "Optimal Discretization of Random Fields," *Journal of Engineering Mechanics*, **119**, pp. 1136–1154 (1993).
15. El-Ramly, H., Morgenstern, N. R. and Cruden, D. M., "Lodalen Slide: A Probabilistic Assessment," *Canadian Geotechnical Journal*, **43**, pp. 956–968 (2006).

(Manuscript received May 14, 2014,
accepted for publication November 13, 2014.)

https://doi.org/10.1017/jmech.2015.5 Published online by Cambridge University Press